Journal of Cell Communication and Signaling (2023) 17:169–188
https://doi.org/10.1007/s12079-022-00685-z

RESEARCH ARTICLE

Prediction of cellular targets in diabetic kidney diseases with single-cell transcriptomic analysis of db/db mouse kidneys

Chenhua Wu[1,2] · Yingjun Tao[2] · Nan Li[1,3] · Jingjin Fei[2] · Yurong Wang[1] · Jie Wu[2] · Harvest F. Gu[1]

Received: 10 March 2022 / Accepted: 21 June 2022 / Published online: 9 July 2022

Abstract

Diabetic kidney disease is the leading cause of impaired kidney function, albuminuria, and renal replacement therapy (dialysis or transplantation), thus placing a large burden on health-care systems. This urgent event requires us to reveal the molecular mechanism of this disease to develop more efficacious treatment. Herein, we reported single-cell RNA sequencing analyses in kidneys of db/db mouse, an animal model for type 2 diabetes and diabetic kidney disease. We first analyzed the hub genes expressed differentially in the single cell resolution transcriptome map of the kidneys. Then we figured out the communication among the renal and immune cells in the kidneys. Data from this report may provide novel information for better understanding the cell-specific targets involved in the aetiologia of type 2 diabetic kidney disease and for cell communication and signaling between renal cells and immune cells of this complex disease.

Keywords Diabetes · Diabetic kidney disease · End-stage renal disease · Proximal epithelial tubularcells · Single-cell RNA sequencing

Abbreviations

AGEs	Advanced glycation end products
ALH	Ascending loop of Henle
BCAA	Branched-chain amino acids
CD-IC	Collecting duct intercalated cell
CD-PC	Collecting duct principal cell
CR	Creatinine
DCT	Distal convoluted tubule
DEGs	Differentially expressed genes
DLH	Descending loop of Hence
DKD	Diabetic kidney disease
DM	Diabetes mellitus
EERA	Erythropoietin receptor
EnC	Endothelial cell
ESKF	End-stage kidney failure
GO	Gene ontology
IDF	International Diabetes Federation
KAP	Kidney androgen-regulated protein
KEGG	Kyoto encyclopedia of genes and genomes
Mac	Macrophage
mtRNA	Mitochondrial RNA
OPN	Osteopontin
PCT	Proximal convoluted tubule
PTCs	Proximal epithelial tubular cells
RAAS	Renin–angiotensin–aldosterone system
RSCEP	Renal stromal cells except PTCs
scRNA-seq	Single-cell RNA sequencing
SNN	Shared nearest neighbor
STZ	Streptozotocin
T1D	Type 1 diabetes
T2D	Type 2 diabetes
tSNE	T-distributed stochastic neighbor embedding
UA	Urinary albuminuria
UAER	Urinary albumin excretion rate

✉ Jie Wu
wujie@cpu.edu.cn

✉ Harvest F. Gu
feng.gu@cpu.edu.cn

[1] Laboratory of Molecular Medicine, School of Basic Medicine and Clinical Pharmacy, China Pharmaceutical University, Nanjing 210009, China

[2] Laboratory of Minigene Pharmacy, School of Life Science and Technology, China Pharmaceutical University, Nanjing 211198, China

[3] Department of Endocrinology, Jiangsu Province Hospital of Traditional Chinese Medicine, The Affiliated Hospital of Nanjing University of Chinese Medicine, Nanjing 210029, China

UMAP	Uniform manifold approximation and projection
UMI	Unique molecular identifiers

Introduction

Diabetes mellitus (DM) is approaching epidemic proportions globally. According to the latest report from the International Diabetes Federation (IDF), approximately 463 million adults (20–79 years) were living with diabetes in 2019, while this will rise to 700 million by 2045 (https://www.idf.org/). Of DM, type 2 diabetes (T2D) is the most common form (more than 90%) and characterized by insulin resistance and abnormalities in insulin production. Diabetic kidney disease (DKD, previously named as diabetic nephropathy) is a microvascular complication and progresses gradually over many years in approximately 50% of patients who are T2D (Thomas et al, 2016). T2D is the leading cause of impaired kidney function, albuminuria, and renal replacement therapy (dialysis or transplantation) worldwide, thus placing a large burden on health-care systems (Thomas et al, 2016, 2015; Doshi & Friedman, 2017). Currently, intensive management of patients with DKD includes controlling blood glucose levels and blood pressure as well as blockade of the renin–angiotensin–aldosterone system (RAAS). Such approaches might show the delayed onset of renal failure, but many patients still progress to end-stage kidney failure (ESKF, also known as end-stage renal disease) despite optimal therapy with the current state of medical care (Thomas et al, 2015; Doshi & Friedman, 2017; Anders et al, 2018). This urgent event requires us to reveal more accurate molecular mechanism of DKD to develop more efficacious treatment in this disease.

Single-cell RNA sequencing (scRNA-seq) analysis can redefine cell types in tissues and identify the cell-type specific changes of gene expression (Tang et al, 2009; Macosko et al, 2015; Zheng et al, 2017). By using this revolutionary technique, the first scRNA-seq analysis in kidneys of C57BL/6 mouse is performed and has generated a comprehensive cell atlas and identified 19 distinct cell types from normal murine kidneys. Approximately 80% of all captured cells are proximal and collecting tubule origin, which highlights the role of the renal tubular system in health and disease (Park et al, 2018). Another scRNA-seq analysis is carried out with glomerular cells isolated from kidneys of streptozotocin (STZ)-induced diabetic endothelial nitric oxide synthase-deficient ($eNOS^{-/-}$) mice and provided the information of the genes expressed differentially in glomerular cells with early DKD (Fu et al, 2019a, b). STZ mouse is widely considered as an animal model for type 1 diabetes (T1D, Furman et al., 2015). In the kidneys of T2D-DKD, however, knowledge of changes of specific cells, particularly in renal tubular cells is still unknown. Herein, we report a scRNA-seq map of kidneys in db/db mice, which is widely accepted as an animal model for T2D and DKD (Sharma et al, 2003). We first identified plenty of markers in proximal tubular cells (PTCs) and other cell clusters in isolated kidney tissues of db/db mice. We then analyzed the hub genes expressed differentially in kidneys of db/db mice in comparison with non-diabetic control mice. Finally, we demonstrated the effect of immune cells, especially T cells, on the whole kidney through cell communication during the DKD process of db/db mice. Thus, the current study may provide novel information for better understanding the cell-specific targets involved in the aetiologia of T2D-DKD.

Results

Cell clusters in kidney tissues of db/db mice

In the isolated kidney tissues from db/db mice, the averaged visible living cells were 841/μl (372–1260/μl). Based upon Findclusters function in Seurat, the clusters of cells were identified by a shared nearest neighbor (SNN) modularity optimization, and the averaged survival rate of all cell clusters was 85.1% (82.0–87.7%). Three-dimension (3D) t-distributed stochastic neighbor embedding (tSNE) maps of PTCs and the rest renal cell types in kidney tissues of db/db mice were severally represented in File S1 and S2. In these 3D interactive HTML images, each cell cluster can be selected by simply clicking the symbol(s) in figure legend. The proportions of all these cell clusters are summarized in Fig. 1A. As you see, the identified cell clusters included ascending loop of Henle (ALH), collecting duct intercalated cell (CD-IC), collecting duct principal cell (CD-PC), distal convoluted tubule (DCT), descending loop of Hence (DLH), endothelial cell (EnC), proximal tubule cells (PTCs), macrophage (Mac), dendritic cell (DC), B and T cells. PTCs were found to be majority of all the cells and proposed by 77.6%. Therefore, PTCs were deservedly singled out and grouped as S1, S2 and S3 according to their segmental regions in proximal tubules of kidneys. To better view the unification of image, PTCs of S1, S2 and S3 segments were selected to be presented in Fig. 1B, while the same image at 3D interactive HTML format was attached in File S1. Except PTCs, the images of other renal cells, including ALH, CD-IC, CD-PC, DCT, DLH and EnC were showed in Fig. 1C, and they were proposed by 13.0%. Furthermore, immune cells, such as Mac, DC, B and T cells were all together occupied by 9.4% (Fig. 1D).

Markers in proximal epithelial tubular cells isolated from kidneys of db/db mice

PTCs in S1, S2 and S3 segments were proportionally grouped and highlighted in orange, green and blue, respectively (Fig. 1B). By using Findmarker function in Seurat,

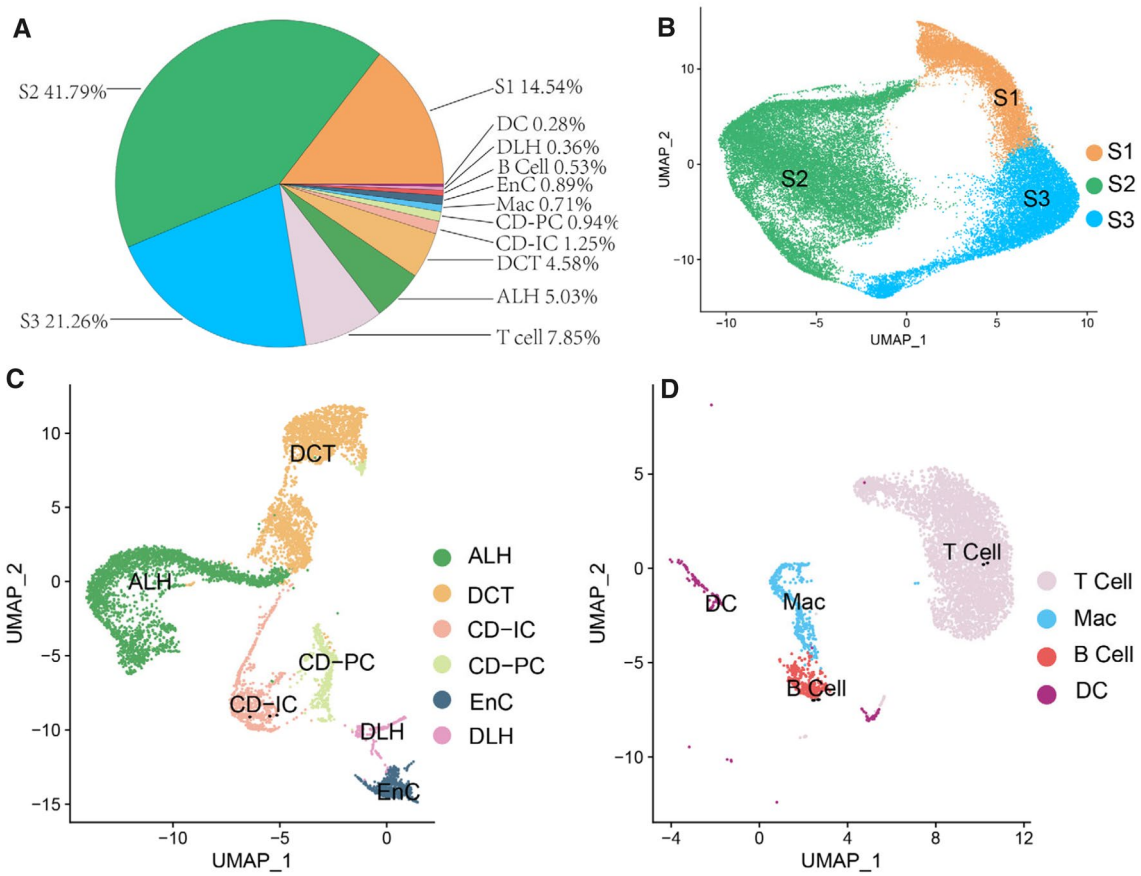

Fig. 1 A pie chart of clusters and proportions of renal and immune cells isolated from kidneys of db/db mice. **A**. Cell clusters and the proportions of each cell cluster are summarized in pie chart. **B**-**D**. Uniform Manifold Approximation and Projection (UMAP) map of PTCs (**B**), renal stromal cells except PTCs (**C**) and immune cells (**D**). Identify clusters of cells by a shared nearest neighbor (SNN) modularity optimization based clustering algorithm. UMAP dimensional reduction technique was performed for cell classification and identification. ALH: Ascending loop of Henle; CD-IC: Collecting duct intercalated cell; CD-PC: Collecting duct principal cell; DCT: Distal convoluted tubule; DLH: Descending loop of Hence; EnC: Endothelial cell; Mac: Macrophage; PTCs: Proximal tubule cells; S1, S2 and S3 are segments of proximal tubule

we further identified 39 markers in PTCs and data were summarized in Fig. S2. To affirm the segmental markers in PTCs, highly specific markers and their expression patterns in PTCs of S1, S2 and S3 segments were represented in Fig. 2A–C. Gene expression patterns in PTCs of S1 and S3 segments were clear and highly separated. Six genes, including *Slc5a2*, *Slc5a12*, *Spp2, Slc6a19, Gatm* and *Slc7a7* were located in S1 segment i.e. early proximal convoluted tubule (PCT). These genes were then considered as markers for PTCs in S1 segment. Another 6 gene, including *Atp11a, Ces1f, Slc6a18, Cyp4a10, Utp20* and *Slc5a8* were found to be highly expressed as markers in late PCT (S3 segment). In PTCs of S2 segment, however, no high-separation marker was observed because the gene expression patterns in PTCs of S2 segment were similar with what in S1 and S3 segments (as seen in Fig. 2B). Biological function of markers in PTCs of S1 and S3 segments and their pathophysiological effects in DKD were summarized in Table 1.

Markers in other cell clusters isolated from kidneys of db/db mice

Except PTCs, the rest cells isolated from kidney tissues of db/db mice (22.4% of all) were identified by SNN modularity optimization based upon clustering algorithm and uniform manifold approximation and projection (UMAP) approach. They were eventually classified as ALH, DCT, CD-IC, CD-PC, Mac, EnC, B and T cells, DLH, DC. Violin plots of top 3 marker genes in these 10 cell clusters were represented in Fig. 2D. The marker gene expression levels in each cell cluster were shown in the violin plots along with no limitation of the same values in horizontal axis, which derived from scale normalized matrix of read counts. Heatmap of marker genes in these cell clusters was demonstrated in Fig. S3. All marker genes of 500 cells (if they are sufficient) of all cell clusters were plotted. High gene expression levels were indicated with yellow while purple

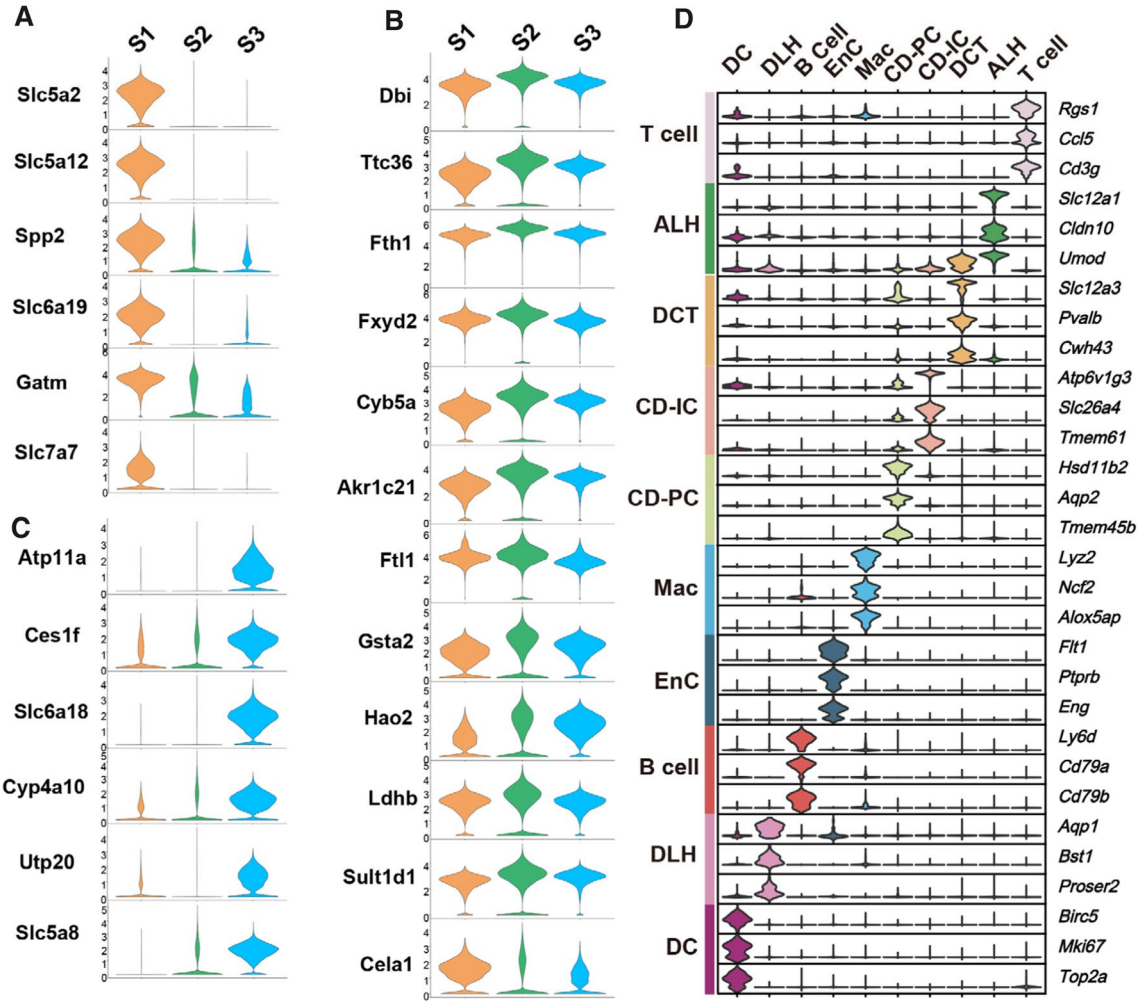

Fig. 2 Marker genes of 13 renal cell types in kidneys of db/db mice. **A**-**C**. The expression of marker genes in S1 (**A**), S2 (**B**) and S3 (**C**) of PTCs was demonstrated in violin plots. **D**. Stacked violin plots represent top 3 marker genes in 10 cell clusters, including T cell, ALH, DCT, CD-IC, CD-PC, Mac, EnC, B cell, DLH and DC. ALH: Ascending loop of Henle; CD-IC: Collecting duct intercalated cell; CD-PC: Collecting duct principal cell; DCT: Distal convoluted tubule; DLH: Descending loop of Hence; EnC: Endothelial cell; Mac: Macrophage; B- and T-cells; DC: Dendritic cells

conversely represents low expression. A list of marker genes of each cell cluster was summarized in Table 2. Information concerning the location of these markers for each cell type may allow us to ensure the accuracy of annotation results and to explore the knowledge for better understanding the molecular mechanisms of DKD.

Genes expressed differentially in renal PTCs between control and db/db mice

Differentially expressed genes (DEGs) in the cell clusters of kidneys between db/db mice with DKD and control mice (Ctrl) were further analyzed. At the same time, we introduced a published data of renal single nuclear RNA sequence (snRNA-Seq) from early DKD patients and control with three each [Wilson PC et al., 2019]. After processing in cell ranger and Seurat similar with the data of mice we produced, a total of 12 cell types including PTC, complement factor H expressing cell (CFH), ALH, DCT, CD-PC, CD-IC, podocyte (PODO), EnC, mesangial cell (MES), T Cell, Mac and B Cell were observed (Fig. S4A-D). We selected cell types that contained more than a hundred cells in both groups for DKD and Ctrl group difference analysis and combined with our mouse data to investigate the linear relationship (Pearson correlation coefficient) of homologous genes in DEG (with significance) according to $\log_2$FC (P adjustment < 0.05 & express percentage $> 20\%$ & $|\log_2 FC| > 1$). Among them, PTC, DCT, CD-IC and EnC showed significant correlation ($R > 0$, $P < 0.05$) in the data of the two species (Fig. S4E). In the data of mice, DEGs in PTCs of S1, S2 and S3 segments with significance were represented in the following heatmaps (Fig. 3A–C). In the

Table 1 Markers in proximal epithelial tubular cells of S1 and S3 segments and their effects in kidneys

Renal cell	Marker	Biofunction	Effects in kidneys
PTC S1 segment	*Slc5a2*	A major cotransporter for sodium-dependent glucose in kidneys	SGLT2 inhibitors block glucose reabsorption in the proximal tubule and improve systemic glucose homeostasis
	Slc5a12	A low-affinity Na(+)-coupled lactate transporter in the initial part of the proximal tubule (S1)	Plasma D-lactic acid levels increased with microalbuminuria and decreased with macroalbuminuria[1]
	Spp2	This gene encodes a secreted phosphoprotein that is a member of the cystatin superfamily	SPP2 is associated with kidney development and maturation in mice. In S1P signaling pathway, it has a strong influence on mesangial cell function and DKD progression[2]
	Slc6a19	This gene encodes a system B(0) transmembrane protein that actively transports most neutral amino acids (especially methionine) across the apical membrane of epithelial cells	The expression level of this gene is correlated with weight loss, improved glucose tolerance and kidney injury degree in mice[3,4]
	Gatm	This gene encodes a mitochondrial enzyme that belongs to the amidinotransferase family. This enzyme is involved in creatine biosynthesis, whereby it catalyzes the transfer of a guanido group from L-arginine to glycine, resulting in guanidinoacetic acid, the immediate precursor of creatine	In renal failure, Gatm forms linear aggregation in proximal tubules, impeding mitochondrial division and leading to mitochondrial degeneration, which eventually leads to renal fibrosis and thickening of basement membrane[5]. Gatm is also associated with serum creatinine content[6]
	Slc7a7	The protein encoded by this gene is the light subunit of a cationic amino acid transporter	*Slc7a7* is a core gene that controls the renal network, and its methylation level plays a key role in the development of DKD[7]
PTC S3 segment	*Atp11a*	The protein encoded by this gene is an intact membrane ATPase, likely to drive the transport of ions (such as calcium) across the membrane	No related report
	Ces1f	Ces1f is a member of the carboxylesterase 1 family and is involved in the breakdown of liver cholesterol esters and triglycerides, thereby participating in fat mobilization [8]	No related report
	Slc6a18	Act as specific transporters for neurotransmitters, amino acids, and osmolytes like betaine, taurine, and creatine	No related report
	Cyp4a10	A member of cytochrome P450	In high glucose environment, *Cyp4a* will lead to ROS production resulting in apoptosis of podocytes. Inhibition of some cytochrome P450 subtypes can prevent the apoptosis of diabetic podocytes and proteinuria[9]
	Utp20	UTP20 is a component of the U3 small nucleolar RNA protein complex and is involved in 18S rRNA processing	No related report
	Slc5a8	This gene functions as a high-affinity sodium-coupled lactate transporter involved in reabsorption of lactate and maintenance of blood lactate level	It could be similar with *Slc5a12*

PTC proximal tubule cell, *Slc5a2* solute carrier family 5 member 2 *Slc5a12* solute carrier family 5 member 12, *Spp2* secreted phosphoprotein 2, *Slc6a19* solute carrier family 6 member 19, *Gatm* glycine amidinotransferase, *Slc7a7 solute carrier family 7 member 7, Atp11a* ATPase phospholipid transporting 11A, *Ces1f*: carboxylesterase 1F, *Slc6a18* solute carrier family 6 member 18, *Cyp4a10* cytochrome P450, family 4, subfamily a, polypeptide 10, *Utp20* UTP20 small subunit processome component, *Slc5a8* solute carrier family 5 member 8

Table 2 Markers in other cells isolated from kidneys and their effects in kidneys

Renal cell	Marker	Biofunction	Effects in kidneys
T cell	*Cd3g*	T cell receptor—part of the CD3 complex. This complex is involved in antigenic recognition coupled to multiple intracellular signal transduction pathways	No related report
	Ccl5	It is a chemokine involved in immune regulation	This proinflammatory mediator may be involved in the recruitment of Mac to attack podocytes[10]
	Rgs1	A regulator of the G protein signaling family	It is associated with IgA nephropathy, CKD, and diabetes mellitus by regulating chemotaxis of immune cells[11]
ALH	*Umod*	Rich in urine, it helps prevent urinary tract infections	In a GWAS study, it was associated with glomerular filtration rate[12]
	Cldn10	Maintains the physical barrier between epithelial and EnC	There is a decrease in the level of transcriptome and DNA methylation in the human PTCs of T2D[13]
	Slc12a1	As sodium–potassium-chloride cotransporter (NKCC2) in ALH	The upregulation of this gene may be related to insulin resistance, pancreatic β-cell dysfunction, and renal diabetes insipidus[14]
DCT	*Pvalb*	Function as Ca^{2+} buffer and Ca^{2+} transporter/shuttle protein	Variants of *Pvalb* may be associated with *Slc12a3*-negative Gitelman's syndrome or similar tubular lesions[15]
	Slc12a3	This cotransporter mediates sodium and chloride reabsorption in DCT	SNPs of SLC12A3 e.g. rs11643718 are associated with the incidence of DKD. High SLC12A3 expression often indicates better renal function[16]
	Cwh43	Related to lipid remodeling during GPI-anchor maturation	It is related to water metabolism, and CWH43 deficiency can lead to brain edema in mice[?]
CD-IC	*Atp6v1g3*	a component of vacuolar ATPase (V-ATPase)	No related report
	Slc26a4	*Slc26a4* (PDS) express in collecting duct intercalated cells (CD-IC) to maintain acid or bicarbonate secretion [17]	Slc26a4 maintains acid–base balance through bicarbonate transport, which is associated with renal tubular acidosis
	Tmem61	A transmembrane protein that transports lipids and cholesterol	No related report
CD-PC	*Hsd11b2*	Hydroxysteroid 11-beta dehydrogenase 2 catalyzes the production of cortisone from glucocorticoid cortisol	Reduced expression of this gene is associated with increased salt sensitivity and hypertension, two DKD traits
	Aqp2	This gene encodes a water channel protein located in the kidney collecting tubule	*Aqp2* expression also prevents renal fibrosis and protects structurally impaired kidneys[18]. Abnormalities in Aqp2 can lead to renal diabetes insipidus
	Tmem45b	Tmem45b is a transmembrane protein, but its clear function is still unknown	No related report
Mac	*Lyz2*	A kind of lysozyme	No related report
	Ncf2	The encoding product is Neutrophil Cytosolic Factor 2, which is an oxidase catalyzing the production of superoxide	No related report
	Alox5ap	It is involved in the synthesis of leukotriene, which mediates various inflammatory responses	The C allele of *ALOX5AP* in rs3803278 plays a renal protective role in Caucasian DKD. The increased expression of this gene is associated with increased glomerular permeability to albumin[19]
EnC	*Flt1*	It belongs to the vascular colorectal growth factor receptor (VEGFR) family and has the activity of tyrosine kinase	In the venous blood of patients with preeclampsia, FLT1 levels are inversely correlated with glomerular filtration rate, and FLT1 is a potential predictor of renal damage[20]
	Ptprb	The gene encodes a member of the protein tyrosine phosphatase (PTP) family, which is involved in the regulation of the cell cycle	No related report
	Eng	Glycoprotein is the main rich glycoprotein in vascular endothelium, which forms part of the transforming growth factor-β receptor complex	The appearance of DKD is often accompanied by the activation of TGF-β signaling pathway

Table 2 (continued)

Renal cell	Marker	Biofunction	Effects in kidneys
B Cell	*Ly6d*	lymphocyte antigen 6 family member D	No related report
	Cd79a	Also known as *IGA*, its coding products are immunoglobulin and B lymphocyte surface antigen components	No related report
	Cd79b	This gene encodes the Ig-beta protein of the B-cell antigen component, which, together with *Cd79a*, is involved in the composition of B lymphocyte antigen receptor and immunoglobulin	No related report
DLH	*Aqp1*	Similar with *Aqp2*, it encodes a transmembrane aquaporin	This gene is responsible for water reabsorption, has increased mRNA and protein levels in diabetes but decreased in DKD with kidney damage[21]
	Bst1	The gene encodes a stromal cell line-derived glycosylphosphatidylinositol-anchored molecule	No related report
	Proser2	Unknown	No related report
DC	*Top2a*	Its encoding product is an enzyme that can change the DNA topological structure and participate in the biological processes such as chromosome concentration, DNA transcription and replication	The content of TOP2A in glomerulus was found to be negatively correlated with creatinine clearance and nephrotic syndrome[22]
	Mki67	This gene encodes a nuclear protein that is involved in cell proliferation	No related report
	Birc5	This gene is a member of the *IAP* gene family and encodes a negative regulatory protein that prevents apoptotic cell death	No related report

Cd3g CD3 antigen, gamma polypeptide, *Ccl5* chemokine (C–C motif) ligand 5, *Rgs1* regulator of G-protein signaling 1, *Umod* uromodulin, *Cldn10* claudin 10, *Slc12a1* solute carrier family 12, member 1, *Pvalb* parvalbumin, *Slc12a3* solute carrier family 12, member 3, *Cwh43* cell wall biogenesis 43 C-terminal homolog, *Atp6v1g3* ATPase, H^+ transporting, lysosomal V1 subunit G3, *Slc26a4* solute carrier family 26, member 4, *Tmem61*, transmembrane protein 61, *Hsd11b2* hydroxysteroid 11-beta dehydrogenase 2, *Aqp2* aquaporin 2, *Tmem45b* transmembrane protein 45b, *Lyz2* lysozyme 2, *Ncf2* neutrophil cytosolic factor 2, *Alox5ap* arachidonate 5-lipoxygenase activating protein, *Flt1* FMS-like tyrosine kinase 1, *Ptprb* protein tyrosine phosphatase, receptor type, B, *Eng* endoglin, *Ly6d* lymphocyte antigen 6 complex, locus D, *Cd79a* CD79A antigen (immunoglobulin-associated alpha), *Cd79b* CD79B antigen, *Aqp1* aquaporin 1, *Bst1* bone marrow stromal cell antigen 1, *Proser2* proline and serine rich 2, *Top2a* topoisomerase (DNA) II alpha, *Mki67* marker of proliferation Ki-67, *Birc5* baculoviral IAP repeat-containing 5

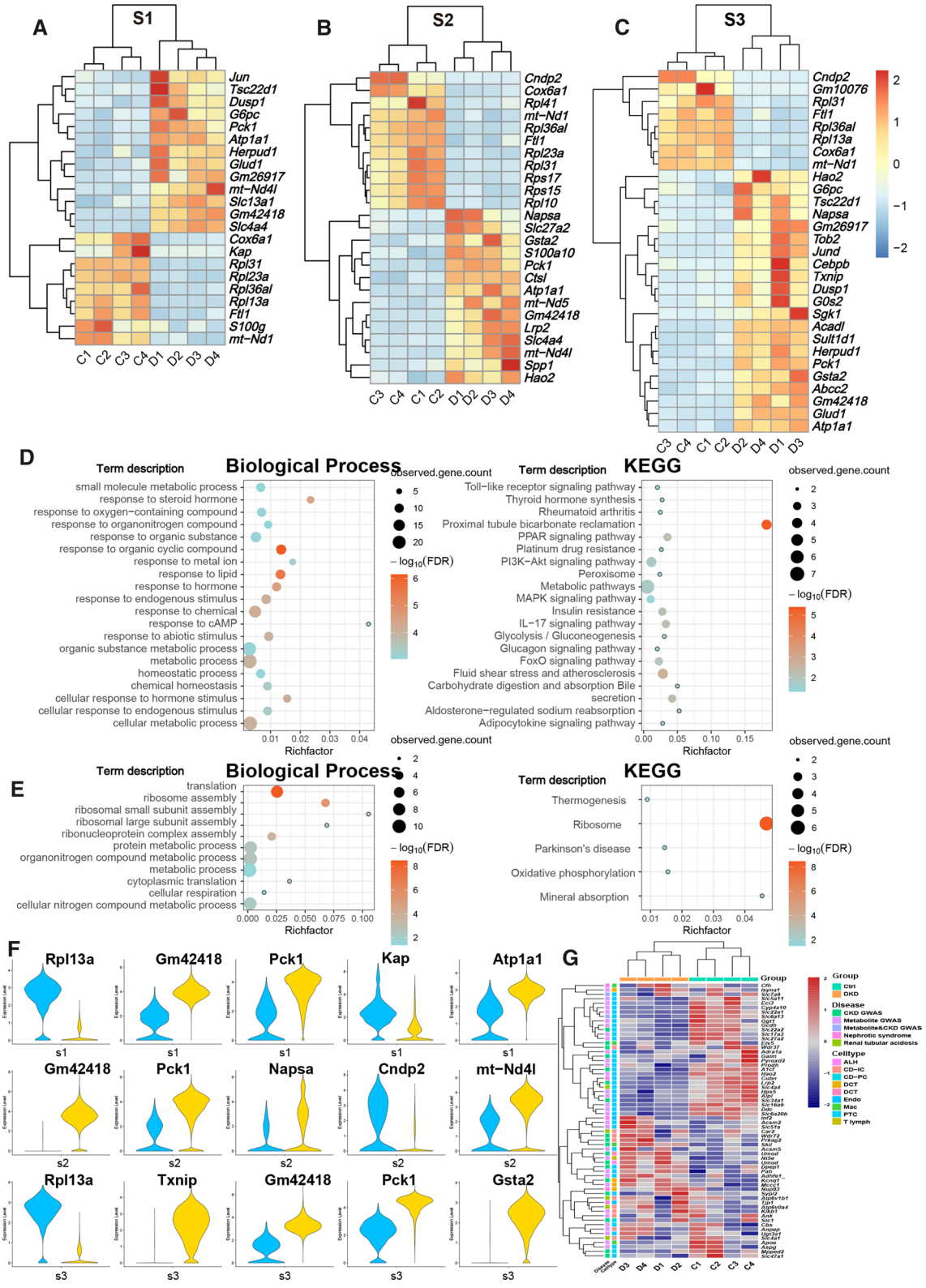

figures, a list of genes was found to be up- or down-regulated in PTCs of the desired segments consistently within the group. As you see, in PTCs of S1, S2 and S3 segments, respectively, the numbers of increased desired DEGs were 13, 14, and 21, while the decreased ones are 9, 11, and 8. Most of DEGs are newly identified, while several reports have evidenced that increased expression of dual specificity phosphatase 1 (*Dusp1*, Fig. 3A and C) and *G0s2* (G0/

◂**Fig. 3** Genes expressed differentially in PTCs of kidneys between db/db and control mice and their biological pathways. **A**-**C**. Genes expressed differentially in PTCs of kidneys between db/db and control mice are summarized. Heatmap depicted DEGs average expression of each sample scaled by rows to display significant difference between two groups PTCs. **D**. The bubble map of enrichment analysis of up-regulated DEGs in S1-3 segments of PTCs in group of DKD showed significant (false discovery rate < 0.05) GO pathway of biological process and KEGG pathway. **E**. It was consistent with the content in D except that the object of enrichment analysis was down-regulated genes. F. Top 5 DEGs of each segmented PTCs according to absolute value of fold change. **G**. Heatmap displayed the expression genes scaled by rows in different groups and cell types

G1 switch 2, Fig. 3C) are involved in the pathogenesis of DKD (Sheng et al, 2019; Zhang et al, 2020; Bai et al, 2019; Ma et al, 2014; Matsunaga et al, 2016). In addition, eight genes including *Pck1*, *Atp1a1*, *Gm42418*, *Cox6a1*, *Rpl31*, *Rpl36al*, *Ftl1* and *mt-Nd1* showed the same difference trend in S1, S2 and S3.

To further explore the function of DEGs set, we achieved KEGG and GO enrichment annotation of up- and down-regulated DEGs, separately (Fig. 3D, E). Biological process pathways obtained from the enrichment of up-regulated genes were mainly concentrated in the response to oxygen-containing compound, steroid hormone, organonitrogen compound and metabolism-related pathways like organic substance metabolic process, metabolic process, and small molecule metabolic process. The most significant KEGG pathway with the highest enrichment factor was PCT bicarbonate reclamation, which is consistent with the main function of PTCs. Moreover, the genes and their related metabolic, glucagon signaling, and glycolysis/gluconeogenesis pathways were also detected (Fig. 3D). Data implicated that three segmented PTCs may fluctuate in material transportation, glucose metabolism and immunological stress. In term of down-regulated gene enrichment analysis, the ribosomal related pathways, including *Rpl31*, *Rpl41*, *Rps17* etc., were annotated in both GO and KEGG enrichments (Fig. 3E).

We selected top 5 DEGs of each segmented PTCs with the largest value according to absolute value of fold change between two groups and they were shown in the violin plots (Fig. 3F). *Kap* and *Pck1* had the same tendency of difference in all three segments of PTCs (Fig. S5A), them are also found to be associated with DKD.

In RSCEP, CD-PC played a dominant role in the pathogenesis of DKD

PTCs, which occupy the largest renal population, has been proved to be involved in the process of DKD above. To clarify whether renal stromal cells except PTCs (RSCEP) is also involved, based upon the predecessors (Park et al, 2018), we collated cell-specific gene sets associated with DKD, metabolite, nephrotic syndrome, and renal tubular acidosis, and then filtered the genes that were significantly different (P adjustment < 0.05) between all cell types of Ctrl and DKD groups. Expression of eligible DEGs in the corresponding cell types between Ctrl and DKD are summarized in Fig. 3G and the multiples, proportions, and significance of genes expression in DKD groups were shown in Table S1 compared with what in Ctrl group. The amount of DEGs in CD-PCs was found to be the highest among all RSCEP (Fig. 4A). To elucidate the dynamic changes of RSCEP in the process of pathology, we conducted trajectory inference (TI) analysis by RNA velocities and results were shown in trajectory profiles, cell accumulation bars, and gradient heat maps (Fig. 4B–K). It can be inferred from TI profiles and cell accumulation bars that the distribution of all types of renal stromal cell types in different pseudotime states with the significant imbalance. Moreover, DEGs expression of renal stromal cell types exhibited in heatmap was changed with the passage of pseudotime and divided into two major clusters. One cluster changed from high to low, while another one went conversely, suggesting that they may embody dynamic damage process during the development of DKD.

We further figured out the top 5 up- and down-regulated DEGs each in CD-PC according to the absolute value of fold changes and the violin figure is shown in Fig. 4L. These 10 genes with the transition of pseudotime changes were also summarized in Fig. 4M. Among them, expression levels of *Atp1a1*, *Spp1*, *Gm42418*, *Calb1*, and *Wnk1* were higher while *Rpl13a*, *Apela*, *Fxyd4*, *Ly6e*, and *mt-Nd1* were lower in DKD compared with Ctrl. Some of these ten genes play their roles in ion transport (eg: *Wnk1*, *Wkn4*, *Fxyd4*), energy production (eg: *Atp1a1*, *mt-Nd1*) and cellular oxidative stress (eg: *Apela*) respectively. Not limited to PTCs, all these gene expression changes suggest that DKD may be a disaster for RSCEP, especially CD-PC.

Cell communication of multiple cell types in kidneys of db/db mice

Traditional bulk RNA-Seq could not explore the interaction of different cell types of kidneys in DKD process. To figure out the potential cellular communication involved in DKD, we used CellChat Packages to calculate the theorical cell communication probability of scRNA-Seq data (Figs. 5 and 6). In the renal cell communication pathway prediction, a total of 2527 interactions were found, among which DKD (2277) contained significantly more than Ctrl (250) contained (Fig. 5A), even considering the difference in the number of cells between groups, the weighted cell communication strength still maintained the same trend. A total of 54 pathways showed significant differences in communication intensity between the two groups. Among them, MK, KIT, CDH5 and PECAM1 pathways, which accounted for a small

A

Cell type	Up-regulation	Down-regulation
S1	13	9
S2	14	11
S3	21	8
ALH	4	10
CD-IC	7	12
CD-PC	16	33
DCT	7	7
DLH	18	14
EnC	4	19
DC	3	13
B Cell	5	15
Mac	15	27
T Cell	14	21

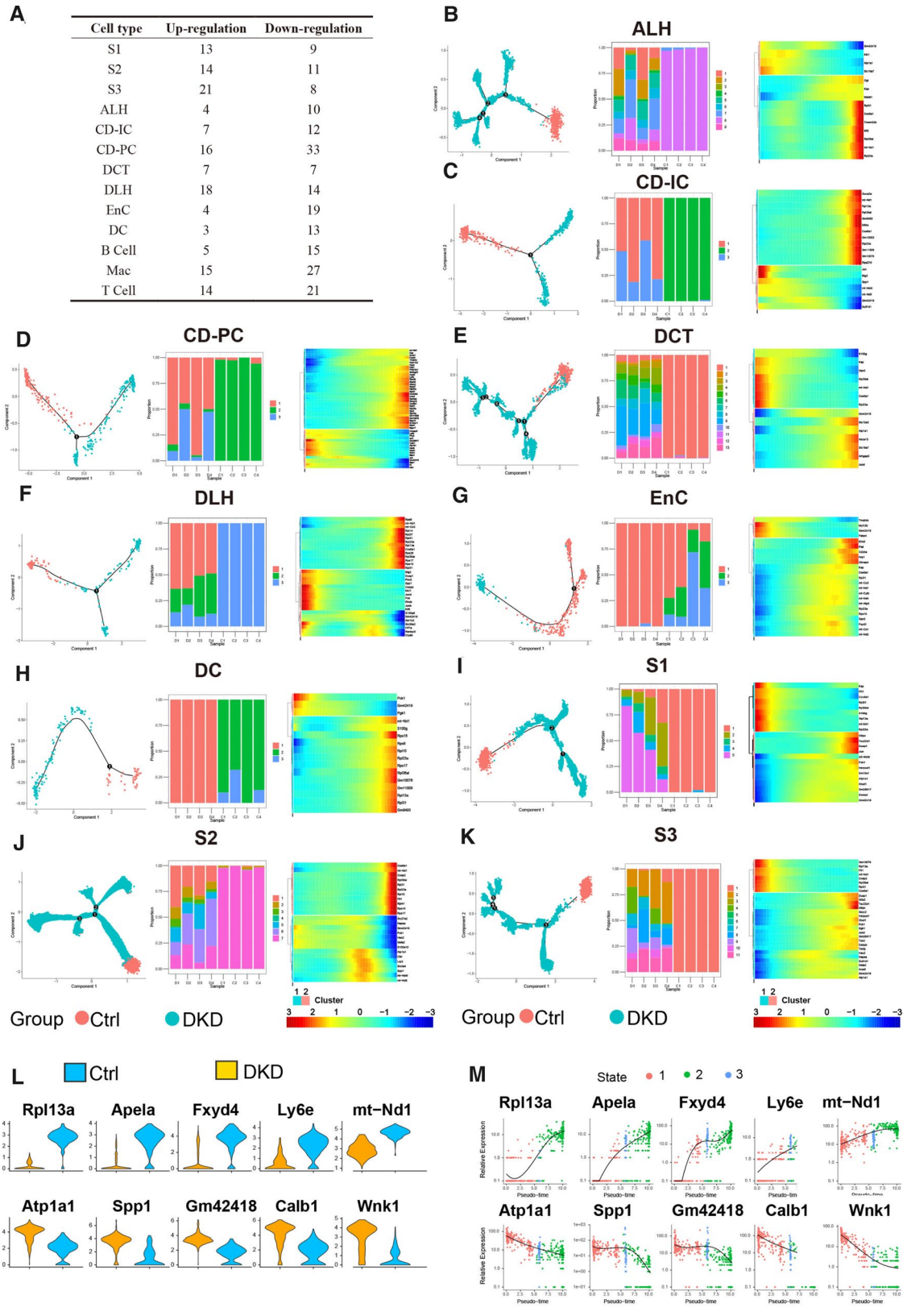

◂**Fig. 4** The cells of DKD group and Ctrl group showed significant differences in Pseudotime analysis. **A**. The table recorded the distribution of both up-regulated and down-regulated DEGs in all renal cells. **B**-**K**. Trajectory inference obtained by Monocle using RNA velocities method. These graphs contain three forms of results severally. The first being, cells were displayed in trajectory dimensionality reduction colored by group. Second, distributions of renal stromal cells in different states among each sample were shown in a percentage bar chart respectively. Third, the heatmap showed gene expression (evaluated by *Z*-value) as the transition during time dynamics of pseudotime. **L**. Top5 up-regulated DEGs and down-regulated DEGs were selected according to the absolute value of fold change generated by the comparison of expression levels between group DKD and group Ctrl in CD-PC. M. Expression of DEGs in Fig. 4E varied during transition with pseudotime states of CD-PC

number of pathways, overpowered DKD in Ctrl. However, the remaining 50 pathways had higher activity in DKD and contain a large number of immune-related pathways such as MHC-I [Jiang NM et al., 2018], CCL [Seo W et al., 2020], IL1 [Mantovani A et al., 2019], IFN-II [Piaszyk-Borychowska A et al., 2019]. Correspondingly, among the four types of immune cells, we found that the incoming intereaction strength of T Cell and the outgoing intereaction strength of Mac increased significantly in DKD, and we have found that these two types of cells were involved in the process of DKD in the difference analysis. Besides, 25 of them have been documented to have explicit relationships with DKD. To verify this result, a similar phenomenon was observed in a previously published human DKD data set, that is, a large number of pathways are activated in DKD and associated with immunity (Fig. S6C). In the human snRNA-Seq data, pathways LAMININ, SPP1, GDF, VISFATIN, CALCR, SEMA3, VCAM and EGF show exactly the same trend on relative information flow as our data (Fig. 5C and Fig. S6C).

Seven communication pathways, including DEGs of the corresponding cell types, were APP, MHC-I, MHC-II, SEMA3, SEMA4, SPP1 and VEGF signaling pathways. The expression levels of DEGs included in signaling pathways among corresponding cell types and groups are represented in Fig. 6B. *Spp1* and *H2-Q7* were up-regulated in DKD, while the others were higher in Ctrl. These cell types involved in the communication pathway of kidneys (Fig. 6C) revealed that these cell types played specific roles (e.g., sender, receiver, mediator) in intercellular information exchange and the color depth of blocks is positively correlated with their importance in cell communication. Chord chart of these pathways widely presented who and how these cell types are connected in cellular communication in Fig. 6D (Only showed the signaling pathways with corresponding DEGs. For example, H2-Q7 as a ligand in DEGs of T Cell, so we only display the corresponding MHC-I pathway exported by T Cell).

Cd74 appeared in APP and MIF pathway as the DEGs of Mac, this gene is upregulated in the renal tubules while the experiment diabetic nephropathy and glomerulonephritis occur (Valiño-Rivas et al, 2015). *Cd74* is positively correlated with inflammatory response and regulates Mac activity by interacting with MHC proteins for antigen presentation. Subsequently, Cd44 and Cd74 are combined to activate a range of immune responses include the secretion of pro-inflammatory cytokines IL-1, IL-2, IL-6, IL-8, INF-C and TNF-α increased by CXCR4 (Su et al, 2017), which is a marker of MIF pathway activation, was also found to be significantly increased in T cell, B cell and Mac of DKD group (Fig. 6F).

Spp1 encodes secreted phosphoprotein 1, which is a kind of Osteopontin (OPN). OPN are usaully expressed in ALH and DLH, but are highly expressed in PTCs under pathological conditions. *Spp1* is also associated with inflammation (Mihai et al, 2019), glomerulosclerosis, tubulointerstitial fibrosis, and nephron loss. In the current study, we found that *Spp1* was one of the five genes that were most up-regulated in CD-PC in DKD. We further analyzed the SPP1 pathway and found that *Spp1* and related genes were up-regulated in all of the cell types in DKD (Fig. S4B). Moreover, the expression levels of *Spp1* were significantly increased in CD-IC, CD-PC, DLH and S2 of PTCs (Fig. 6B). Cd44, as a receptor of Spp1, was found up-regulated in Mac of DKD (Fig. 6B). Generally, the expression of *Cd44* is low in kidneys of healthy individuals, but high in the subjects with renal diseases (Crisi et al, 2009). Furthermore, the activation of Cd44 can cause the recruitment, invasion and phagocytosis of Mac and neutrophils (Patouraux et al, 2017). Thereby, Mac may extensively infiltrate and attack the kidney due to the increased expression of *Spp1* in renal stromal cells, and eventually cause nephritis injury.

Mac is generally regarded as the etiological core of many inflammatory diseases including DKD (Fu et al, 2019a, b). In the current study, we found that Mac and T cells were involved in MHC I and II communications, respectively. To a large extent, the inflammatory characteristics of Mac come from their plasticity in different stages of the inflammatory response, resulting in different phenotypes and specificity in the diverse stimulation, disease, tissue and inflammation (Stables et al, 2011). From Fig. 6D (MHC I and II signaling network), we can roughly see that Mac had an effect on all renal cells by acting on T cells. *Il1b*, *Nfkb1* and *Nlrp3* can be used as biomarkers for Mac activation, so the expression of these activation signals was higher in group DKD (Fig. 6E) also showed that Mac initiated inflammatory response in DKD. Moreover, *Il1b* is a marker for M1 cells, suggesting M1 is the dominant subtype of Mac in DKD (there are two subtypes of Mac in total: M1 and M2. M1 primarily act as a pro-inflammatory role and M2 play an anti-inflammatory role). APP, MIF, SPP1, MHC I and II pathways all proved that Mac, in particular, is the culprit of immune cells in the

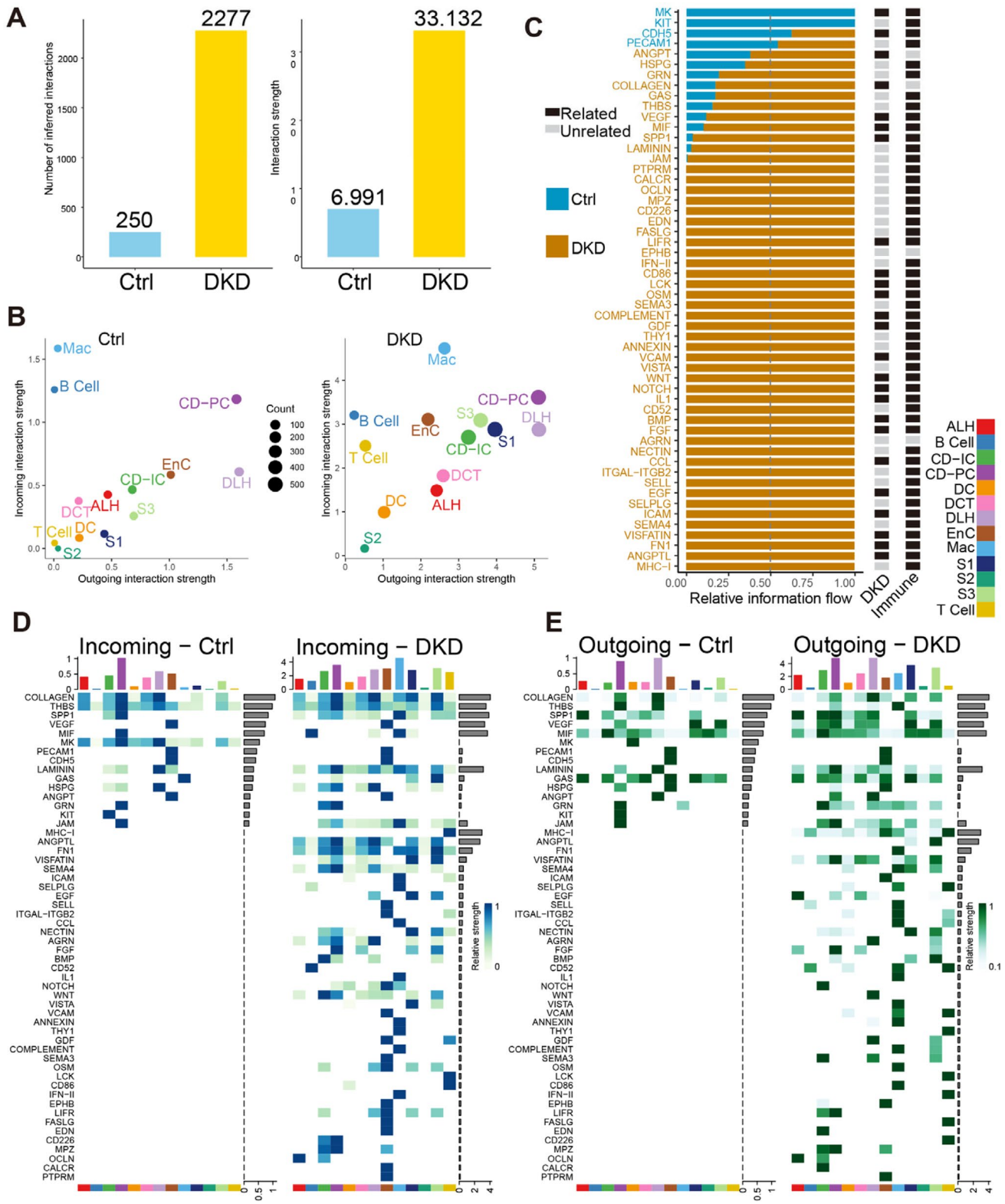

inflammatory response of DKD and may play the role of initiator in DKD-inflammation rather than B and T cells. This conjecture is intuitively drawn in the schematic diagram (Fig. 6H).

We found that down-regulation of *Nrp1* was extensively involved in the communication of renal cells (Fig. 6A). This mechanism may be related to the binding of Nrp1 to Vegfa and the affinity of Vegfr2 (*Kdr*), the receptor of Vegfa, in

◂**Fig. 5** Global differences in cell communication pathways were observed between Ctrl and DKD groups. **A**. Histogram of the number and the weighted strength of cell interactions calculated by Cellchat in Ctrl (blue) and DKD (yellow). **B**. The bubble diagram showed the outgoing and incoming interaction strenth comparison of 13 renal cell types in Ctrl and DKD respectively. **C**. All significant cell communication signaling pathways were ordered based on differences of relative information flow between Ctrl and DKD. Blue represents the Ctrl-riched pathway and yellow represents the DKD-riched pathway. Black and gray represent whether there is direct documentary evidence of immunity and DKD. D-E: Identify signals contribution of outgoing and incoming signaling pathways within Ctrl (**D**) and DKD (**F**) groups were depicted by complex heatmap

EnC (Fig. 6G). Data from the current study clearly shown that *Nrp1* was lost in EnC of DKD group (Fig. 6B). At the same group, *Vegfa* levels in many cell types were increased (Fig. 6G) and all of them acted on EnC by Kdr (Fig. 6D). In other words, even though the ligand (*Vegfa*) and receptor (*Kdr*) expression of the VEGF pathway was high in DKD group, the signaling pathway could not be activated effectively because of the lack of *Nrp1*.

Variation of DKD in the perspective of gene sets

To better understand the changes of related gene sets rather than individual gene in kidney cell types and immune cells of DKD, we performed Gene Set Variation Analysis (GSVA) based upon the expression matrix of each cell type. According to KEGG, GSEA and PubMed, the 52 gene sets related to DKD are summarized in Table S2. The GSVA scores for each sample were presented in the Table S3. A total of 34 gene sets including lysine degradation, oxidative phosphorylation, TGF-β and ROS generation etc. were found to have significant differences among various cells between DKD and Ctrl groups (Fig. 7A). On one hand, T Cell, ALH and DCT cells contained the largest number of differential gene sets among 13 cell types (Fig. 7B–D). On another hand, lysine degradation, oxidative phosphorylation, TGF-β, and valine, leucine and isoleucine biosynthesis gene sets appeared most frequently with significance in various cell types (Fig. 7E–H).

From the cellular point of view, we found that ALH had 13 different gene sets (Fig. 7C). Significantly, this largest number of gene sets was related to amino acid metabolism such as valine, leucine, isoleucine, and scored higher in DKD. Moreover, the scores of TCA cycle, ROS generation and hypoxia gene sets were both higher in the pathological condition, which indicated that ALH in DKD was subjected to more severe oxidative stress state and there might be oxidative phosphorylation coupling disorder. Hyperglycemia-related advanced glycation end products (AGEs) can activate the AGE/RAGE pathway and further induce oxidative stress, chronic inflammation, and nitrogen production. Data from the current study implicated that activation of the AGE/RAGE gene set of T cell was accompanied by activation of the PI3K/Akt/mTOR, Nitrogen metabolism and Autophagy gene set of DCT. On the other hand, the activation of Notch signaling pathway can induce the differentiation fate of CD cells, and ultimately lead to the increase in CD-PC in CKD. This is consistent with what T cell could accelerate the disease course (Figs. 5B and 6D and H).

The gene sets in relation with Lysine degradation, Oxidative phosphorylation, TGF-β, and Valine, leucin and isoleucine biosynthesis showed the most significant occurrences in various cell types (Fig. 7E–H). TGF-β is an important factor reflecting the level of inflammation and fibrosis in DKD (Du et al, 2020). TGF-β gene set had higher GSVA score in T cell, B cell, Mac, S1 and EnC of DKD group (Fig. 7G). In the metabolism-related pathways, biosynthesis of valine, leucine, and isoleucine has higher scores in six types of DKD cells, and in our unpublished metabolomic data, the content of these three branched-chain amino acids (BCAA) has indeed increased significantly in the DKD group. Elevated BCAA levels may indicate higher levels of insulin resistance and dysoxidation of fatty acids.

Discussion

We have used scRNA-seq to analyze transcriptome differences in db/db mice with DKD compared with non-diabetic control mice from the cell image at single cell resolution. In bioinformatics analyses, we made cell annotation based upon the previous studies. Results from the current study provides several markers available for renal cell identification and clustering. Researchers are welcomed to use the TransferData function in Seurat to classify your query cells based upon our Seurat object as reference data.

In further analyses, our data demonstrate that the expression matrix of PTCs is changed in a specific pattern, including inflammatory response, substance metabolism, oxidative stress, hormone regulation and material transport during the DKD process. KEGG and GO enrichments of DEGs in PTCs suggest that PPAR (Kim & Park, 2019), MAPK (Yang et al, 2016), PI3K-AKT (Wang et al, 2019), TNF and Toll – like receptor signaling pathways may be involved in the pathogenesis of DKD (Fig. 3D–E). What has long been overlooked is that disruption of ribosomal gene expression (Fig. 3E) may cause the compensatory renal hypertrophy (Northrup et al, 1977) and this phenomenon was observed in HE stained sections of kidney tissues (Fig. S1C-D). Moreover, we found eight genes are similarly altered in the course of disease in all three PTCs, for instance, kidney androgen-regulated protein (KAP) is a proximal tubule androgen-regulated gene. Up-regulation of *Kap* could maintain glucose metabolism homeostasis, improve hypertension, proteinuria, and focal segmental glomerulosclerosis (de Quixano et al,

A

Gene	As DEGs in	Pathway Name	Identity
H2-Aa	Mac	MHC-II	Ligand
H2-Ab1	Mac	MHC-II	Ligand
H2-DMa	Mac	MHC-II	Ligand
H2-Eb1	Mac	MHC-II	Ligand
Cd74	Mac	MIF	Receptor
H2-Q7	T Cell	MHC-I	Ligand
Spp1	CD-IC, CD-PC, DLH, S2	SPP1	Ligand
Nrp1	EnC	SEMA3, SEMA4, VEGF	Receptor

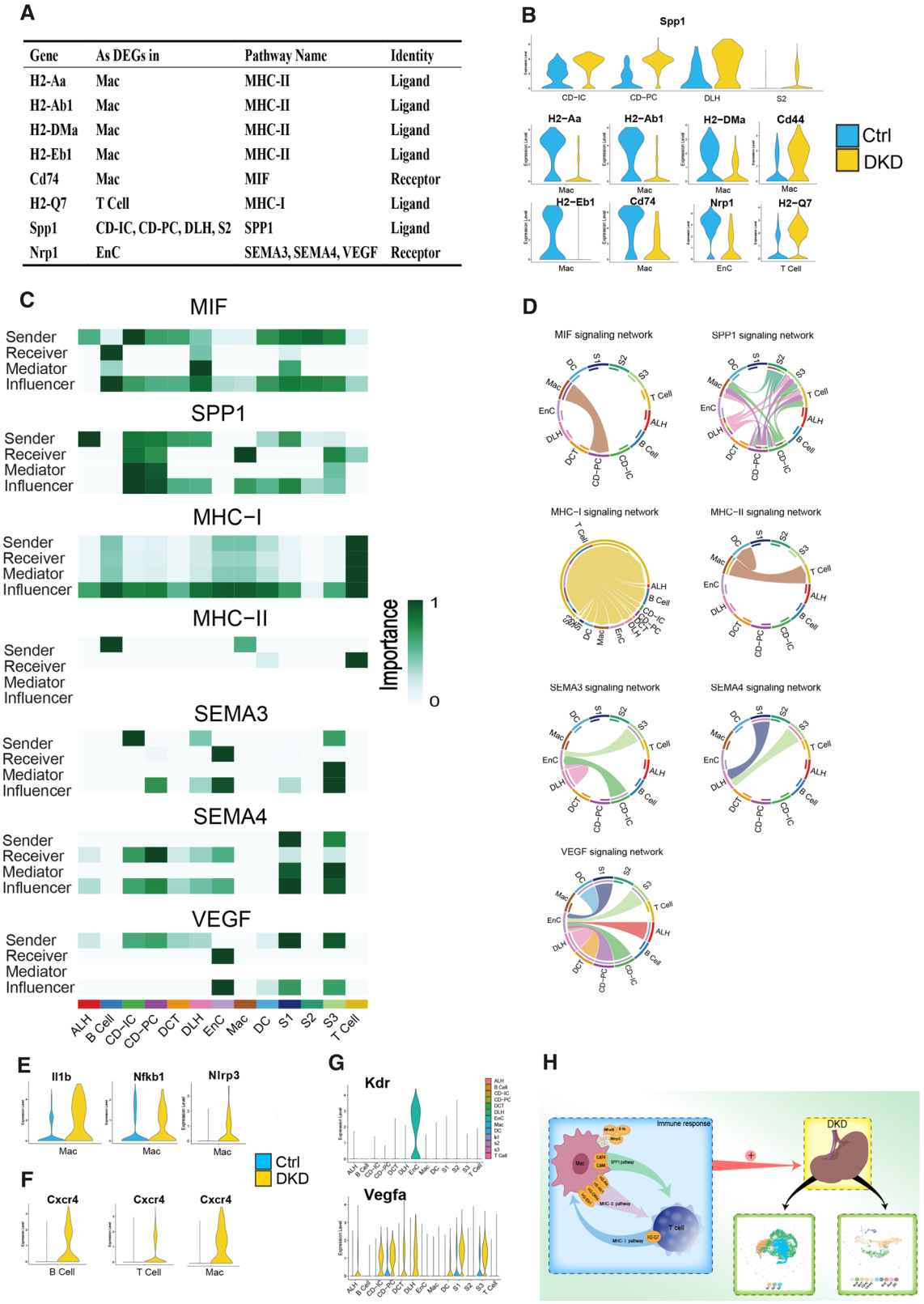

2017). *Pck1* encodes cytosolic isozyme of phosphoenolpyruvate carboxykinase (PEPCK-C), and this gene is associated with T2D (Beale et al, 2007). *Kap* expression was found to be consistently increased in 3 segmented PTCs (Fig. 3F), while *Pck1* was decreased in 3 segmented PTCs (Fig. 3F). This finding suggested that *Kap* and *Pck1* dysfunction may

◂**Fig. 6** Cell communication in kidneys of db/db mice. **A**. The table shows the names of cell signaling pathways, source cell types and roles that DEGs participated in cell communication. B. The expression levels of DEGs involved in cell communication in corresponding cells between the two groups. C. Calculative contribution and importance of each ligand-receptor pair to the overall communication, which reflect the total communication role of every cell type in these signaling pathways by heatmap. D. Intercellular signaling pathways of these DEGs were displayed in chord chart. E–G. Violin diagram of genes related to upstream or downstream of DEGs. F. Schematic diagram of T Cell and Mac participating in Cell communication in DKD process

be involved in pathogenesis of kidney injury in DKD. This also indicates that the cells of these three segments of PTCs are similarly affected in the process of DKD.

Besides PTCs, we have analyzed other cells and TI data showed dynamic changes in all renal stromal cells during the development of DKD (Fig. 4). This may not only contribute to the discovery of cell-specific predictors in DKD, but also help us to determine the predictor thresholds. In this process the DEGs of CD-PC reveals that it has been subjected to drastic effects, for example, With-no-lysine kinases (WNKs) regulate electrolyte transport in renal tubules to maintain potassium homeostasis. *Wnk1* and *Wnk4* are key regulatory factors of NCC (*Slc12a3*), which can increase sodium reabsorption in kidneys and lead to the decrease of potassium transport in downstream nephritic units. One previous study has demonstrated that expression of *WNK1*, *WNK4* and *ATP1A1* is increased in human CD-PC with terminal DKD, which is accompanied by an increase in potassium secretion, an increase in serum creatinine and proteinuria (Boyd-Shiwarski et al, 2017). Another study with microarray approach has revealed up-regulated inclusion of *Calb1* in the kidneys of mice with DKD (Zhang et al, 2020). The key gene *Calb1*, together with Kim-1, Cystatin C and albumin, covers the most severe injury sites in kidneys and is recommended as a marker of renal injury (Fuchs & Hewitt, 2011). FXYDs are single span membrane proteins (Sweadner et al, 2003) and five members of this family can regulate the affinity between Na–K-ATPase and sodium ions. *Fxyd2* increases the affinity of Na–K-ATPase (eg, *Slc12a1* and *Slc12a3*) to potassium ions on the surface of the cell, conversely, *Fxyd4* helps the sodium ions bond (Crambert & Geering, 2003). Loss of *Fxyd2* could further lead to increased glucose tolerance, incremental circulating insulin levels and the absence of IR. Reduction of *Fxyd4* in mRNA level reflects the rapid, dramatic appearance of impaired kidney function. Expression levels of *Fxyd4* in Ctrl group were significantly higher (4.00 times, Fig. 4L) and the expression level of *Fxyd2* in DKD group was significantly higher (1.8 times, Table S1). Thus, there may be a disruption of the natrium-potassium transport balance in CD-PC when the kidney is exposed to DKD. In an in vitro study, apoptosis, inflammatory response, mitochondrial ROS, DNA damage in NRK-52E renal tubular epithelial cells accompanied by decreased expression level of *Apela* which encodes a renal petide hormone (ELABELA). However, the addition of exogenous ELABELA can inhibit DNA damage and apoptosis, especially the regulation of C-caspase-related pathways (Li et al, 2020). In another in vivo trial of mice, 5 consecutive days of Lipopolysaccharides (LPS) administration resulted in a decrease in *Apela* levels and impaired renal function as indicated by an increase in serum creatinine and an increase in proteinuria levels (Xu et al, 2020). From another point of view, treatment with ELABELA can reverse these changes by reducing nephritis, ROS, and apoptosis. All these data indicate that the expression of *Apela* in CD-PC is crucial for the maintenance of normal kidney function. In the current study, we found that this gene was down-regulated in group DKD (Fig. 4L), which is a pessimistic signal for CD-PC in DKD. Briefly, DEGs of CD-PC between DKD and Ctrl groups are mainly manifested as the disruption of the balance of sodium and potassium transport and the increase of the production of pro-inflammatory factors and ROS. These demonstrate that CD-PC was the cell type most affected by DKD except for PTCs.

About cell communication in DKD process, the SPP1 pathway was found to be widely activated in CD-IC, CD-PC, DLH and S2 of PTCs (Fig. 6B–D). High expression of OPN is known to be associated with proteinuria, reduced creatinine clearance rate, fibrosis, macrophage and T cell infiltration, as one of them, *Spp1* is no exception (Kaleta, 2019). In addition to immune factors, the activation of *Spp1* in high glucose environments leads to the transformation of renal energy source from β-oxidation to glycolysis pathway, which ultimately leads to ROS production and renal tubulointerstitial fibrosis (Shirakawa & Sano, 2020). In another pathway, balance of the VEGFA/VEGFR system in EnC cells is necessary for normal glomerular development and mature renal homeostasis. The upregulation of this inversely correlated marker with albuminuria is associated with vascular rarefication and renal fibrosis. It has been found that the activation of this pathway in DKD in EnC is caused by the communication with neighboring EnC and podocytes (Fu et al, 2019a, b). In current study, we also found that all renal stromal cells expressed high levels of *Vegfa* in DKD and acted on *Vegfr* (*Kdr*) of EnC to achieve abnormal activation of this pathway (Fig. 6D and G), but immune cells were not involved at all. In terms of angiogenesis, we found that the ligand (*Vegfa*) of VEGF pathway was increased in the DKD group and the receptor (*Kdr*) was increased in EnC. Through cellular communication analysis, we revealed that there is a strong interaction between Nrp1, Vegfa and Vegfr2. Nrp1 can combine with Vegfa-$_{164}$/Vegfa-$_{A165}$ to increase the affinity between Vegfa and Vegfr2, so Nrp1 is a necessary condition for the activation of angiogenesis signaling pathway. The reduced expression of *Nrp1* may directly reduce the

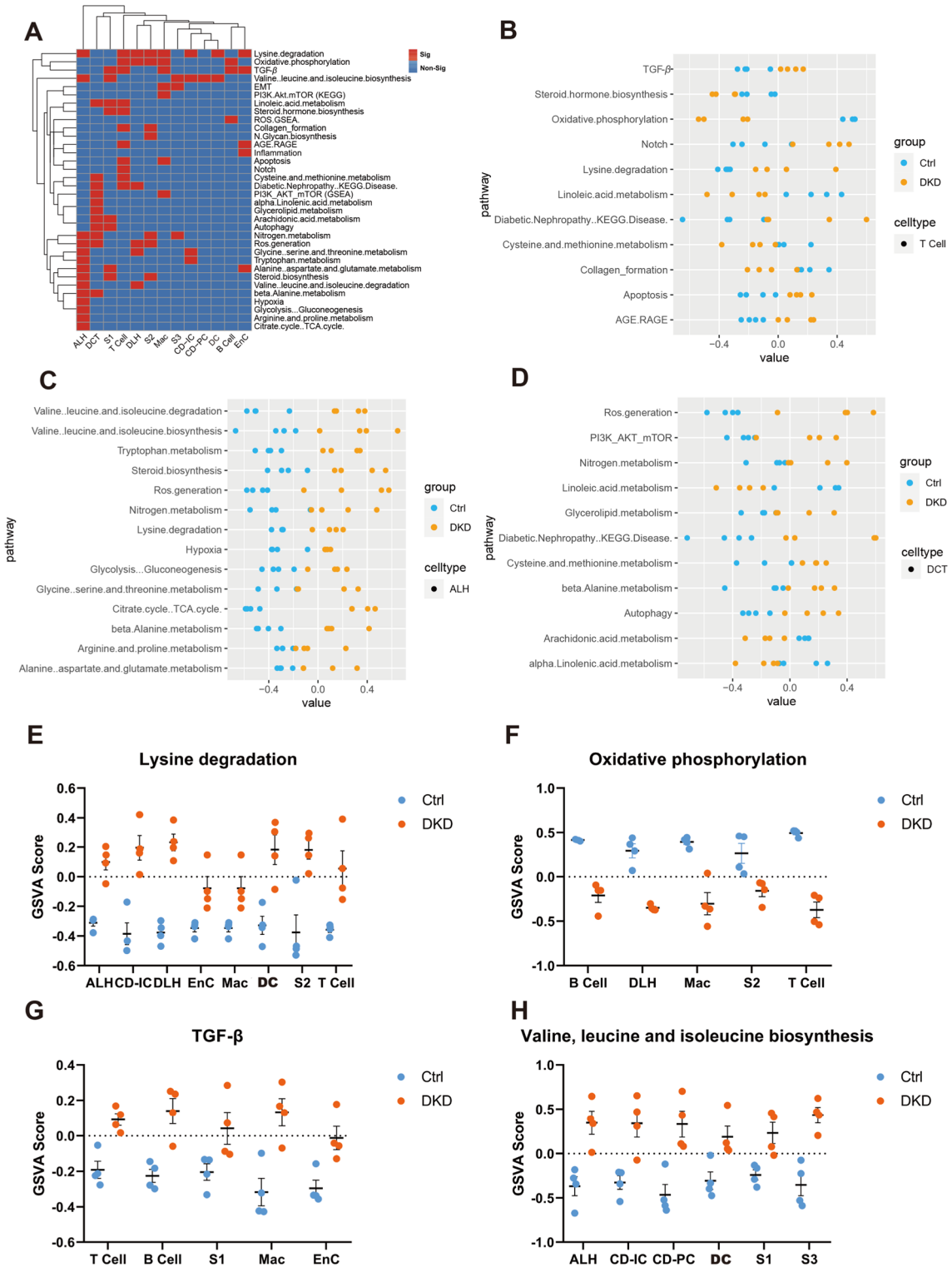

Fig. 7 GSVA analysis in various types of renal cells. **A**. Heat map showed whether levels of DKD-related gene sets differ significantly between the two groups in the corresponding cells. Red represents significance ($P<0.05$) and blue represents non-significance. **B**-**D**. The dot plot showed the GSVA results of T cell, ALH and DCT in DKD-related gene sets of each sample in group DKD and group Ctrl. E–H. GSVA scores plot of Lysine degradation, Oxidative phosphorylation, TGF-β, valine, leucine and isoleucine biosynthesis gene sets were displayed by each sample (P-values are both greater than 0.01 and less than 0.05, so no additional annotation was made in the figures)

adhesion ability between cells, leading to the destruction of the glomerular filtration barrier (Bondeva & Wolf, 2015). Considering that vascular tissues are rich in kidneys, the blocking of this angiogenesis and cell adhesion pathways is undoubtedly devastating.

Among immune cells, cellular communication pathways such as SPP1, MIF, MHC-I and MHC-II well charge with the role of Mac especially M1 in immune attack on renal stomal cells. Under the DKD condition, the dominant M1 in Mac can not only directly attack renal stromal cells through the SPP1 pathway, but also activate T cells through the MHC-II pathway, which in turn can further identify other renal cells through the MHC-I pathway. We indeed observed a significant increase in the intensity of outgoing pattern of Mac and incoming pattern of T Cell in DKD in global cell communication (Fig. 5B).

Limitations

ScRNA-seq is an intricate technique, and there are limitations, such as sequencing coverage bias and low capture efficiency. During the preparation of single-cell suspension, cell breakage, loss of cytoplasmic RNA and contamination of mitochondrial DNA may occur in the experiments. In the current study, we failed to capture and isolate the podocytes from kidneys of db/db mice because the number of podocytes is small. Thereby, there is no information concerning podocytes in this report. To fully dissect the complexity of DKD, further investigation of podocytes by using appropriate research approach has been taken into our consideration. Due to differences in species, trial batches, and techniques, there is no complete agreement on gene expression and cell type between our data of mice set and publicly available human data set (Fig. S4 & Fig. S6).

In conclusion, the current study of scRNA-seq with db/db mouse kidneys expands our understanding of renal cells in DKD in terms of oxidative stress, metabolism, immune homeostasis, and material transport and provides a large number of hub DEGs and pathways, which can be used for further investigation of the pathophysiological process in DKD.

Material and methods

Animals

BKS.Cg-Dock7m $^{+/+}$ Leprdb/J (db/db) mice (group DKD) aged 6 weeks were obtained from Cavens Laboratory Animal Co. Ltd, China. All experiments with the mice were performed in accordance with the guideline of, and were approved by, the Institutional Animal Care and Use Committee at China Pharmaceutical University. All mice were male and housed in plastic cages with a controlled environment (22–25˚C; 40–50% humidity; and 12-h light/dark cycle) and free access to regular chow and water. Body weight and blood glucose levels of the mice were monitored weekly by glucometer readings. DM was confirmed with blood glucose levels greater than 16.7 mmol/L (Fig. S1A). After then, mice were placed in metabolic cages weekly to collect urine for 24 h. Concentrations of urinary albuminuria (UA) were detected with ELISA quantitative kits (Elabscience Biotechnology, USA). Urinary albumin excretion rates (UAER) values in DKD mice from 11 to 21 week were significantly higher than what in Ctrl (Fig. S1B).

Animal experiment procedures were approved by the Experimental Animal Ethical Committee of China Pharmaceutical University, and in accordance with the criteria described in the NIH Guide for the Care and Use of Laboratory Animals.

Preparation of kidney RNA library

The left kidneys of 4 db/db mice were harvested for single-cell sequencing analyses. To avoid the damage of renal cells caused by the lysis of red blood cells, a cardiac perfusion protocol was used to remove red blood cells before kidney extraction during the preparation of single-cell suspension. The harvested kidneys were dissociated to single-cell suspension with multi-tissue dissociation kit 1 (Miltenyi Biotec, Germany) and examined with a microscope after 0.4% Trypan blue coloring. Samples with a survival rate of more than 80% were selected and the cell concentrations were adjusted to 1000/μl for RNA library preparation with ChromiumTM controller and ChromiumTM single-cell 3' reagent version 2 kits (10xGenomics Inc., USA).

Histological analysis of kidneys

The specimens of right kidneys of mice for light microscope assessment were fixed in 10% neutral buffered formalin, embedded in paraffin, and cut into 4-μm-thick sections and stained with H&E reagent. Histology of diabetic kidneys was examined with a light microscope (Olympus, Japan). We randomly selected 5 fields from renal HE sections of each mouse for semi-quantification of glomerular area, interstitial area of glomerulus, and ratio of vacuolar and staining area (Fig. S1E-G) using Image-Pro Plus (Version 6.0.0.260).

ScRNA-seq analyses

After reverse transcription in single-cell gel bead in emulsions, cDNA library including barcode, unique molecular identifiers (UMI) and sample index was stored in drikold. ScRNA seq analyses were completed with DNBseq platform (BGI, Wuhan Technology Center, China).

The current scRNA-Seq analyses generated 169 GB of data. An average of 31,510.14 reads in each cell were detected, while 2,196.45 genes examined. A minimum cell survival rate coloring with 0.4% Trypan blue is summarized in Table S4. According to the cell survival rate, the mitochondrial filtration parameter was determined to be 22% for quality control. After then, 58,259 cells were divided into 13 clusters by Findclusters function for the downstream visualization. High-quality marker genes belong to each cluster were completed as shown in Fig. S2-3.

Bioinformatics

FASTAQ files of scRNA-seq data were split according to sample index. Barcode filtering was used to obtain RNA reads (cDNA insert). RNA reads were then projected onto the mouse genome from NCBI (assembly GRCm38.p5) using STAR (Version 2.4.2a) during the construction of 10X genomic standard output file produced by the Cellranger (Version 5.0.1) in Ubuntu (16.04.6 LTS). Seurat (Version 3.0.2) were used to process the downstream data (8) and the followed visualization process in R (Version 4.0.2) was performed. The regression of mitochondrial RNA (mtRNA) was performed after dimensionality reduction analysis and visualization of clusters was done by using the UMAP method. In addition, scRNA-seq data of 4 male C57BL/6 mice kidneys were adopted from NCBI GEO database (GSE107585) for no batch effect integration as a control group. In the process of de-batching, after our and reference data were processed into normalized expression matrix, the FindVariableFeature function is used to figure out the top 2000 variable genes for anchor calculation between data sets. Finally, de-batch integration of data is achieved through the canonic correlation analysis using Integrate Data function in Seurat.

Subset function to control the quality of each cell (nFeature_RNA > 200 & nFeature_RNA < 6000 & percent.mt < 22) was then used. After processing the data by LogNormalize and ScaleData algorithm, the FindVariableFeature function was applied to screen out feature gene for subsequent Principal Component Analysis (PCA). The first 20 PCAs were selected to find Cluster function. Dimensionality reduction analysis and visualization of clusters were carried out with the UMAP method. FindAllMarkers function was further used for identification of the cell types of clusters. The top high-quality marker gene of each cluster was selected with VlnPlot function analysis, and annotated through capturing from two databases, mouse cell atlas (9) and cell marker (10). The annotated clusters were re-named, and all cells were re-clustered after isolation of PTCs.

To profile detailed cell numbers and the differentially expressed genes (DEGs) between three groups, some kinds of cells, such as immune cell, PTCs were selected out in Subset for re-analysis. DEGs of corresponding cluster between three groups were filtered by Findmarker function while screening criteria were cell expression percentage > 20% and adjustment P value < 0.05. Subsequently, Kyoto Encyclopedia of Genes and Genomes (KEGG) and Gene Ontology (GO) enrichment information of DEGs obtained by clusterProfile (Version 4.0.5). After that, KEGG and GO enrichment bubble diagram was prepared using ggplot2 packages in R. Pseudotime analysis of Ctrl to DKD was done through Monocle (Version 2.0.1) so that the TI results were obtained. The cell communication is done by referring to the entire CellChatDB.mouse via a function in CellChat (Version 1.0.0). Finally, GSVA was be handled by the R package GSVA (Version 1.36.3). The mouse DEGs were converted by the convert_mouse_to_human_symbols function in nichenetr (Version 1.1.0), and the linear relationship between the mouse DEGs and the human DEGs was fitted by lm function, at the same time the Person coefficient was calculated. The computation of human cell communication is consistent with the partial processing of mice except that the database is CellChat.human.

Materials and methods

Reagent/Resource	Reference or source	Identifier or catalog number
Experimental models		
Mouse: C57	Jackson Lab	C57BL/6 J; Cat# JAX:000,664, RRID:IMSR_JAX:000,664
Mouse: db/db	Cavens Laboratory Animal Co. Ltd, China	BKS.Cg-Dock7m + /+ Leprdb/J (db/db); Cat# 2,669,928, RRID:MGI:2,669,928
Reagent kit		
MAU ELISA Kit	Elabscience Biotechnology	E-EL-M0792c
Cr ELISA Kit	Elabscience Biotechnology	E-EL-0058c
multi-tissue dissociation kit 1	Miltenyi Biotec	Cat# 130–110-203
Trypan blue	Biosharp	BL707A
ChromiumTM single-cell 3' reagent version 2 kits	10xGenomics Inc	PN-1000075
Software/Package		

Reagent/Resource	Reference or source	Identifier or catalog number
Cellranger	10X Genomics	RRID:SCR_021002; https://github.com/10XGenomics/cellranger
Seurat	satijalab	RRID:SCR_007322; https://satijalab.org/seurat/
clusterProfile	YuLab-SMU	https://github.com/YuLab-SMU/clusterProfiler
Monocle2	cole-trapnell-lab	RRID:SCR_016339; http://cole-trapnell-lab.github.io/monocle-release/docs/
CellChat	sqjin	https://github.com/sqjin/CellChat
ggplot2	r-project	RRID:SCR_014601; https://cran.r-project.org/web/packages/ggplot2/index.html
GSVA	bioconductor	RRID:SCR_021058; https://www.bioconductor.org/packages/release/bioc/html/GSVA.html
Other		
DNBseq platform	BGI	RRID:SCR_011114; http://www.genomics.cn/en/

Supplementary Information The online version contains supplementary material available at https://doi.org/10.1007/s12079-022-00685-z.

Acknowledgements The authors wish to thank Dr. Katalin Susztak for her positive agreement and valuable discussion.

Authors' contributions Conceived and designed the experiments: Harvest F. Gu; Data acquisition and analysis: Chenhua Wu, Yingjun Tao, Nan Li, Jingjin Fei; Laboratory management: Yurong Wang; Data interpretation: Jie Wu, and Harvest F. Gu; Manuscript preparation and revision: Chenhua Wu and Harvest F. Gu; All authors agreed and approved the final version of manuscript.

Funding This study was supported by the start grants from China Pharmaceutical University (CPU20180815 HFG), the Cooperation Research Project (CPU20200228 HFG).

Data availability The datasets and computer code produced in this study are available in the following databases: Our scRNA-Seq data: Sequence Read Archive PRJNA749372 (https://www.ncbi.nlm.nih.gov/sra/PRJNA749372). In order to provide scRNA profiles from this study, we have constructed an interactive shiny-app as a web tool for your visit (http://biomamba.com:34038/DKD.data.set/). Referenced scRNA-Seq data: Gene Expression Omnibus GSE107585 (https://www.ncbi.nlm.nih.gov/geo/query/acc.cgi?acc=GSE107585). Other original contributions are included in this article, including tables, figures, and supplementary material.

Declarations

Conflict of interests The authors declare no competing interests.

Consent for publication The authors of the manuscript have read and agreed to the consent for publication.

References

Anders HJ, Huber TB, Isermann B, Schiffer M (2018) CKD in diabetes: diabetic kidney disease versus nondiabetic kidney disease. Nat Rev Nephrol 14(6):361–377

Bai M, Chen H, Ding D, Song R, Lin J, Zhang Y, Guo Y, Chen S, Ding G, Zhang Y et al (2019) MicroRNA-214 promotes chronic kidney disease by disrupting mitochondrial oxidative phosphorylation. Kidney Int 95:1389–1404

Beale EG, Harvey BJ, Forest C (2007) PCK1 and PCK2 as candidate diabetes and obesity genes. Cell Biochem Biophys 48:89–95

Bondeva T, Wolf G (2015) Role of neuropilin-1 in diabetic nephropathy. J Clin Med 4:1293–1311

Boyd-Shiwarski CR, Shiwarski DJ, Roy A, Namboodiri HN, Nkashama LJ, Xie J, McClain KL, Marciszyn A, Kleyman TR, Tan RJ et al (2017) Potassium-regulated distal tubule WNK bodies are kidney-specific WNK1 dependent. Mol Biol Cell 229:499–509

Crambert G, Geering K (2003) FXYD proteins: new tissue-specific regulators of the ubiquitous Na,K-ATPase. Sci Signal 2003(166):re1–re1. https://doi.org/10.1126/scisignal.1662003re1

Crisi GM, Marconi SA, Rockwell GF, Braden GL, Campfield TJ (2009) Immuno-localization of CD44 and osteopontin in developing human kidney. Pediatr Res 65:79–84

de Quixano BB, Villena JA, Aranda M, Brils G, Cuevas A, Hespel T, Lekuona H, Súarez C, Tornavaca O, Meseguer A (2017) Kidney androgen-regulated protein (KAP) transgenic mice are protected against high-fat diet induced metabolic syndrome. Sci Rep 7:16102

Doshi SM, Friedman AN (2017) Diagnosis and management of Type 2 diabetic kidney disease. Clin J Am Soc Nephrol 12:1366–1373

Du Y, Yang YT, Tang G, Jia JS, Zhu N, Yuan WJ (2020) Butyrate alleviates diabetic kidney disease by mediating the miR-7a-5p/P311/TGF-β1 pathway. FASEB J 34:10462–10475

Fu J, Akat KM, Sun Z, Zhang W, Schlondorff D, Liu Z, Tuschl T, Lee K, He JC (2019a) Single-Cell RNA profiling of glomerular cells shows dynamic changes in experimental diabetic kidney disease. J Am Soc Nephrol 30:533–545

Fu J, Lee K, Chuang PY, Liu Z, He JC (2019b) Glomerular endothelial cell injury and cross talk in diabetic kidney disease. Am J Physiol Renal Physiol 308:F287-297

Fuchs TC, Hewitt P (2011) Biomarkers for drug-induced renal damage and nephrotoxicity-an overview for applied toxicology. AAPS J 13:615–631

Furman BL (2015) Streptozotocin-induced diabetic models in mice and rats. Curr Protoc Pharmacol. https://doi.org/10.1002/0471141755.ph0547s70

Jiang NM, Cowan M, Moonah SN, Petri WA Jr (2018) (2018) The impact of systemic inflammation on neurodevelopment. Trends Mol Med 24(9):794–804

Kaleta B (2019) The role of osteopontin in kidney diseases. Inflamm Res 68:93–102

Kim Y, Park CW (2019) Mechanisms of adiponectin action: implication of adiponectin receptor agonism in diabetic kidney disease. Int J Mol Sci 20:1782

Li Y, Huang J, He S, Lu Z, Zhang J, Li X, Yang Z, Hoffman RM, Wu Q (2020) APELA/ELA32 Reduces iodixanol-induced apoptosis,

inflammatory response and mitochondrial and dna damage in renal tubular epithelial cells. Anticancer Res 40:635–643
Ma T, Lopez-Aguiar AG, Li A, Lu Y, Sekula D, Nattie EE, Freemantle S, Dmitrovsky E (2014) Mice lacking G0S2 are lean and cold-tolerant. Cancer Biol Ther 15:643–650
Macosko EZ, Basu A, Satija R, Nemesh J, Shekhar K, Goldman M, Tirosh I, Bialas AR, Kamitaki N, Martersteck EM et al (2015) Highly Parallel Genome-wide Expression Profiling of Individual Cells Using Nanoliter Droplets. Cell 161:1202–1214
Mantovani A, Dinarello CA, Molgora M, Garlanda C (2019) Interleukin-1 and related cytokines in the regulation of inflammation and immunity. Immunity 50(4):778–795
Matsunaga N, Ikeda E, Kakimoto K, Watanabe M, Shindo N, Tsuruta A, Ikeyama H, Hamamura K, Higashi K, Yamashita T et al (2016) Inhibition of G0/G1 switch 2 ameliorates renal inflammation in chronic kidney disease. EBioMedicine 13:262–273
Mihai S, Codrici E, Popescu ID, Enciu AM, Rusu E, Zilisteanu D, Necula LG, Anton G, Tanase C (2019) Inflammation-related patterns in the clinical staging and severity assessment of chronic kidney disease. Dis Markers 2019:1814304
Northrup TE, Irwin D, Malt RA (1977) Ribosomal proteins of mouse kidney: normal status and during compensatory renal hypertrophy. Mol Cell Biochem 17:25–30
Park J, Shrestha R, Qiu C, Kondo A, Huang S, Werth M, Li M, Barasch J, Suszták K (2018) Single-cell transcriptomics of the mouse kidney reveals potential cellular targets of kidney disease. Science 360:758–763
Patouraux S, Rousseau D, Bonnafous S, Lebeaupin C, Luci C, Canivet CM, Schneck AS, Bertola A, Saint-Paul MC, Iannelli A et al (2017) CD44 is a key player in non-alcoholic steatohepatitis. J Hepatol 67:328–338
Piaszyk-Borychowska A, Széles L, Csermely A, Chiang HC, Wesoły J, Lee CK, Nagy L, Bluyssen HAR (2019) Signal integration of IFN-I and IFN-II With TLR4 involves sequential recruitment of STAT1-complexes and NFκB to enhance pro-inflammatory transcription. Front Immunol 10:1253
Seo W, Shimizu K, Kojo S, Okeke A, Kohwi-Shigematsu T, Fujii SI, Taniuchi I (2020) Runx-mediated regulation of CCL5 via antagonizing two enhancers influences immune cell function and anti-tumor immunity. Nat Commun 11(1):1562
Sharma K, McCue P, Dunn SR (2003) Diabetic kidney disease in the db/db mouse. Am J Physiol Renal Physiol 284:F1138-1144
Sheng J, Li H, Dai Q, Lu C, Xu M, Zhang J, Feng J (2019) DUSP1 recuses diabetic nephropathy via repressing JNK-Mff-mitochondrial fission pathways. J Cell Physiol 234:3043–3057
Shirakawa K, Sano M (2020) Sodium-glucose Co-transporter 2 inhibitors correct metabolic maladaptation of proximal tubular epithelial cells in high-glucose conditions. Int J Mol Sci 21:7676
Stables MJ, Shah S, Camon EB, Lovering RC, Newson J, Bystrom J, Farrow S, Gilroy DW (2011) Transcriptomic analyses of murine resolution-phase macrophages. Blood 118:e192-208
Su H, Na N, Zhang X, Zhao Y (2017) The biological function and significance of CD74 in immune diseases. Inflamm Res 66:209–216
Sweadner KJ, Arystarkhova E, Donnet C, Wetzel RK (2003) FXYD proteins as regulators of the Na, K-ATPase in the kidney. Ann N Y Acad Sci 986:382–387
Tang F, Barbacioru C, Wang Y, Nordman E, Lee C, Xu N, Wang X, Bodeau J, Tuch BB, Siddiqui A et al (2009) mRNA-Seq whole-transcriptome analysis of a single cell. Nat Methods 6:377–382
Thomas MC, Brownlee M, Susztak K, Sharma K, Jandeleit-Dahm KAM, Zoungas S, Rossing P, Groop PH, Cooper ME (2015) Diabetic kidney disease. Nat Rev Dis Primers. https://doi.org/10.1038/nrdp.2015.18
Thomas MC, Cooper ME, Zimmet P (2016) Changing epidemiology of type 2 diabetes mellitus and associated chronic kidney disease. Nat Rev Nephrol 12:73–81
Valiño-Rivas L, Baeza-Bermejillo C, Gonzalez-Lafuente L, Sanz AB, Ortiz A, Sanchez-Niño MD (2015) CD74 in kidney disease. Front Immunol 6:483
Wang Y, Lu YH, Tang C, Xue M, Li XY, Chang YP, Cheng Y, Li T, Yu XC, Sun B et al (2019) Calcium dobesilate restores autophagy by inhibiting the VEGF/PI3K/AKT/mTOR signaling pathway. Front Pharmacol 10:886
Wilson PC, Wu H, Kirita Y, Uchimura K, Ledru N, Rennke HG, Welling PA, Waikar SS, Humphreys BD (2019) The single-cell transcriptomic landscape of early human diabetic nephropathy. Proc Natl Acad Sci USA 116(39):19619–19625
Xu F, Zhou H, Wu M, Zhang H, Zhang Y, Zhao Q, Brown R, Gong DW, Miao L (2020) Fc-elabela fusion protein attenuates lipopolysaccharide-induced kidney injury in mice. Biosci Rep 40:BSR20192397
Yang XH, Pan Y, Zhan XL, Zhang BL, Guo LL, Jin HM (2016) Epigallocatechin-3-gallate attenuates renal damage by suppressing oxidative stress in diabetic db/db mice. Oxid Med Cell Longev 2016:2968462
Zhang Y, Li W, Zhou Y (2020) Identification of hub genes in diabetic kidney disease via multiple-microarray analysis. Ann Transl Med 8:997
Zheng GX, Terry JM, Belgrader P, Ryvkin P, Bent ZW, Wilson R, Ziraldo SB, Wheeler TD, McDermott GP, Zhu J et al (2017) Massively parallel digital transcriptional profiling of single cells. Nat Commun 8:14049